Science Advances
AAAS

Supplementary Materials for

Dominance of benthic fluxes in the oceanic beryllium budget and implications for paleo-denudation records

Kai Deng *et al.*

Corresponding author: Kai Deng, kai.deng@erdw.ethz.ch

Sci. Adv. **9**, eadg3702 (2023)
DOI: 10.1126/sciadv.adg3702

This PDF file includes:

Supplementary Text

Estimation of continent ^{10}Be input to the oceans

The oceanic external ^{10}Be input includes atmospheric wet and dry deposition at the ocean surface, eolian dust, the riverine dissolved load, and a benthic flux via diagenetic release from continent-derived sediments. The major sink is scavenging onto marine particles, as for ^{9}Be. We consider atmospheric deposition as the sole dominant external source given the very small magnitude of other ^{10}Be sources. Here we aim to validate this assumption based on some simple calculations.

The atmospheric ^{10}Be deposition at the ocean surface (*5.77 ± 1.41 mol/yr*) is calculated by multiplying the global-average atmospheric ^{10}Be depositional flux (*41*) by the global ocean area. The effective riverine dissolved ^{10}Be input to the oceans is derived following three steps. 1) The atmospheric deposition to the global river basins (1.56 ± 0.38 mol/yr) is calculated as the product of the global-average atmospheric ^{10}Be depositional flux and the global drainage area (*57*), which sets the upper limit for continent-derived (dissolved and particulate) ^{10}Be input to the oceans. 2) Global riverine dissolved [^{10}Be] (~320 ± 80 at/g) can be estimated by partitioning atmospheric ^{10}Be input into two components: the dissolved (river water) and particulate (river sediment) forms. Specifically, this partitioning is based on global water and sediment discharge data (*57*) and a Be partition coefficient (1.5×10^5 L/kg) (*58*) estimated from global discharge-weighted water pH (7.1) (*59*). 3) Hence, the effective riverine ^{10}Be input to the oceans (*0.009 ± 0.002 mol/yr*) is the product of the global riverine dissolved [^{10}Be], the global water discharge and the fraction of ^{10}Be escaping the estuarine trap (44%; same as ^{9}Be; (*14*)). The dust ^{10}Be input (*0.15 ± 0.05 mol/yr*) is calculated as the product of the global dust flux (*38)* and dust [^{10}Be] represented by that in loess from the Chinese Loess Plateau (*60*), assuming that 100% of dust ^{10}Be is soluble, to yield an upper-limit estimate.

To estimate the diagenetic release of ^{10}Be from continent-derived terrestrial particles that mainly occurs on continental shelves, we first derive a global-average riverine sediment $(^{10}Be/^{9}Be)_{reac}$ ($1.2 \pm 0.6 \times10^{-9}$ at/at) based on its relationship with denudation rates (*61*) and the global average denudation rate of 233 t/km^2/yr (*57*). Next, we estimate the benthic flux of ^{10}Be on continental shelves (*0.05 ± 0.04 mol/yr*) as the product of the $(^{10}Be/^{9}Be)_{reac}$ above and the benthic ^{9}Be flux on continental shelves (Table S5). This might be an upper-limit estimate for the benthic ^{10}Be flux from terrestrial particles, because a small fraction of the shelf benthic Be flux might be sourced from the marine authigenic fraction rather than the terrestrial authigenic fraction (*49*).

To conclude, the effective continental ^{10}Be input to the oceans is only ~0.21 mol/yr, and thus the atmospheric deposition accounts for 96.5% of the total external ^{10}Be input to the oceans. Considering that the relative uncertainty of atmospheric ^{10}Be deposition is 20-30%, adding or excluding other sources only slightly changes the estimate of the total external ^{10}Be input. Hence, we consider atmospheric deposition as the sole oceanic ^{10}Be source for simplification in the main text.

Table S1. Basic characteristics of sampling stations

Station	Continental margin	Longitude	Latitude	Water Depth	Bottom water O_2[1]
		°E	°N	m	μmol/L
C6-1	East China Sea	122.0	31.1	6	304
C10	East China Sea	122.5	31.0	12	306
C13	East China Sea	122.9	30.8	33	115
B14	East China Sea	122.9	30.1	46	203
AL543-8	Baltic Sea	10.2	54.5	23	<0.1
AL543-12	Baltic Sea	10.1	54.6	24	36
Soledad	Mexico margin	-112.7	25.2	542	<0.1
Catalina	California margin	-118.6	33.3	1300	19
San Clemente	California margin	-118.1	32.6	2053	52
Patton Escarpment	California margin	-120.6	32.4	3707	132

Note: 1) Bottom water O_2 data on the East China Sea shelf and the Mexico-California margins are from (*50*) and (*26*), respectively.

Table S2. Pore-water Be, Mn and Fe concentrations[1,2,3,4]. Stations are shown in Table S1.

Station	Basin	Core depth cm	Be pM	Mn μM	Fe μM
C6-1	East China Sea	0	76.9	0.0	<D.L.
C6-1	East China Sea	1	130.2	4.9	<D.L.
C6-1	East China Sea	2	154.0	40.0	<D.L.
C6-1	East China Sea	4	165.4	47.6	<D.L.
C6-1	East China Sea	7	256.4	77.7	<D.L.
C6-1	East China Sea	9	255.8	99.5	<D.L.
C6-1	East China Sea	11	279.6	92.6	0.0
C6-1	East China Sea	17	411.4	110.3	0.0
C6-1	East China Sea	21	549.0	112.9	95.2
C10	East China Sea	0	46.3	<D.L.	0.0
C10	East China Sea	1	110.1	83.0	<D.L.
C10	East China Sea	3	166.5	75.3	<D.L.
C10	East China Sea	4	160.8	110.6	<D.L.
C10	East China Sea	6	193.7	162.7	0.1
C10	East China Sea	7	296.2	131.0	25.4
C10	East China Sea	9	343.8	73.0	211.1
C10	East China Sea	12	407.7	92.5	299.9
C10	East China Sea	16	401.2	89.8	337.6
C10	East China Sea	25	402.9	51.4	99.3
C13	East China Sea	0	45.8	0.0	0.1
C13	East China Sea	1	142.7	118.7	0.2
C13	East China Sea	2	278.7	162.3	94.7
C13	East China Sea	3	264.0	167.5	106.3
C13	East China Sea	4	268.6	92.1	105.2
C13	East China Sea	7	253.4	28.2	43.8
C13	East China Sea	9	225.0	26.0	60.1
C13	East China Sea	11	228.8	19.2	28.7
C13	East China Sea	17	222.4	21.9	22.8
C13	East China Sea	21	194.8	18.4	10.3
B14	East China Sea	0	54.8	0.0	<D.L.
B14	East China Sea	1	129.0	9.3	0.1
B14	East China Sea	2	282.2	20.0	30.5
B14	East China Sea	5	136.8	34.1	21.8
B14	East China Sea	6	222.3	46.9	55.2
B14	East China Sea	7	152.5	34.9	10.7
B14	East China Sea	9	156.2	27.6	3.7
B14	East China Sea	11	153.4	23.2	3.6
B14	East China Sea	15	145.1	20.3	5.9
B14	East China Sea	19	212.7	21.0	26.2
AL543-8	Baltic Sea	0	89.9	14.9	2.1
AL543-8	Baltic Sea	0.5	162.7	30.4	0.6

AL543-8	Baltic Sea	1.5	259.8	43.8	0.5
AL543-8	Baltic Sea	2.5	485.9	61.3	0.8
AL543-8	Baltic Sea	3.5	608.0	70.0	0.3
AL543-8	Baltic Sea	4.5	691.3	66.4	1.0
AL543-8	Baltic Sea	5.5	613.4	58.7	0.3
AL543-8	Baltic Sea	7	725.8	52.2	0.2
AL543-8	Baltic Sea	9	683.0	46.5	0.3
AL543-8	Baltic Sea	11	933.5	42.5	0.6
AL543-8	Baltic Sea	13	652.6	37.9	0.3
AL543-8	Baltic Sea	16	667.4	29.7	0.6
AL543-8	Baltic Sea	20	775.4	23.3	0.7
AL543-12	Baltic Sea	0	57.5	0.6	2.0
AL543-12	Baltic Sea	0.5	474.0	43.2	60.8
AL543-12	Baltic Sea	1.5	660.4	48.2	16.6
AL543-12	Baltic Sea	2.5	852.7	53.0	1.5
AL543-12	Baltic Sea	3.5	774.7	52.1	0.6
AL543-12	Baltic Sea	4.5	766.2	61.4	0.3
AL543-12	Baltic Sea	5.5	960.3	65.4	0.7
AL543-12	Baltic Sea	7	630.5	73.9	0.4
AL543-12	Baltic Sea	9	651.8	66.0	0.3
AL543-12	Baltic Sea	11		50.0	0.3
AL543-12	Baltic Sea	13	863.1	43.7	0.5
AL543-12	Baltic Sea	16	884.0	36.1	0.3
AL543-12	Baltic Sea	20	969.4	42.6	0.5
Soledad	Mexico margin	0.5	23.0	0.1	63.2
Soledad	Mexico margin	1.5	30.7	0.2	45.7
Soledad	Mexico margin	2.5	57.4	0.1	38.4
Soledad	Mexico margin	3.5	44.9	0.1	9.1
Soledad	Mexico margin	4.5	44.7	0.1	3.3
Soledad	Mexico margin	5.5	61.4	0.1	2.6
Soledad	Mexico margin	6.5	47.5	0.1	1.1
Soledad	Mexico margin	7.5	51.9	0.0	0.6
Soledad	Mexico margin	8.5	48.4	0.0	0.4
Soledad	Mexico margin	9.5		0.0	0.4
Catalina	California margin	0.5	16.8	3.3	0.0
Catalina	California margin	1.5	85.6	13.8	11.0
Catalina	California margin	2.5	110.9	6.1	19.0
Catalina	California margin	3.5	63.9	4.4	23.6
Catalina	California margin	4.5	87.8	3.5	24.9
Catalina	California margin	5.5	132.7	3.3	28.6
Catalina	California margin	6.5	109.4	3.4	30.4
Catalina	California margin	7.5	47.6	3.4	24.5
Catalina	California margin	8.5	83.5	3.0	23.0
Catalina	California margin	9.5	66.8	2.9	23.9

San Clemente	California margin	0.5	50.3	0.3	0.0
San Clemente	California margin	1.5	41.9	3.0	0.1
San Clemente	California margin	2.5	48.0	30.6	0.2
San Clemente	California margin	3.5	37.4	44.9	0.2
San Clemente	California margin	4.5	52.1	56.8	0.2
San Clemente	California margin	5.5	49.5	66.8	1.1
San Clemente	California margin	6.5	46.2	75.5	4.8
San Clemente	California margin	7.5	47.9	81.8	7.9
San Clemente	California margin	8.5	42.1	88.2	8.5
San Clemente	California margin	9.5	87.2	94.1	7.8
Patton Escarpment	California margin	0.5	52.2	0.0	<D.L.
Patton Escarpment	California margin	1.5	16.3	0.0	<D.L.
Patton Escarpment	California margin	2.5	47.5	0.0	<D.L.
Patton Escarpment	California margin	3.5	96.6	0.1	<D.L.
Patton Escarpment	California margin	4.5		1.0	0.1
Patton Escarpment	California margin	5.5	36.5	7.3	0.1
Patton Escarpment	California margin	6.5	34.9	11.2	0.1
Patton Escarpment	California margin	7.5	46.6	13.2	0.1
Patton Escarpment	California margin	8.5	41.1	13.2	0.1
Patton Escarpment	California margin	9.5		15.2	0.1

Note: 1) A relative uncertainty of 10% is applied for all element measurements.
2) <D.L.: below detection limit.
3) All element concentrations were measured at ETH Zürich using Element XR, except Mn data in the Baltic Sea that were measured at GEOMAR (Germany) using ICP-OES.
4) Fe-Mn concentration data from the East China Sea was previously reported in (*50*).

Table S3. Diffusive sedimentary Be fluxes from this study and the literature

Station	Basin	Lat.	Long.	Water depth	T[1]	Be gradient[2]	Uncertainty	D_{Be}^{sed}[3]	Diffusive Be flux[3]	Uncertainty[4]	Reference
		°N	°E	m	°C	pmol/L/cm	pmol/L/cm	cm^2/s	$pmol/cm^2/yr$	$pmol/cm^2/yr$	
C6-1	East China Sea	31.1	122.0	6	25	53.3	15.1	5.01E-06	7.6	2.2	This study
C10	East China Sea	31.0	122.5	12	25	63.7	11.9	5.01E-06	9.1	1.7	This study
C13	East China Sea	30.8	122.9	33	25	116.5	14.1	5.01E-06	16.6	2.0	This study
B14	East China Sea	30.1	122.9	46	25	113.7	14.4	5.01E-06	16.2	2.0	This study
AL543-8	Baltic Sea	54.5	10.2	23	14	158.4	19.8	3.69E-06	16.6	2.1	This study
AL543-12	Baltic Sea	54.6	10.1	24	13	833.1	95.5	3.62E-06	85.5	9.8	This study
Soledad	Mexico margin	25.2	-112.7	542	4	10.8	2.6	2.59E-06	0.8	0.2	This study
Catalina	California margin	33.3	-118.6	1300	4	36.9	6.1	2.59E-06	2.7	0.4	This study
San Clemente	California margin	32.6	-118.1	2053	4	39.9	11.7	2.59E-06	2.9	0.9	This study
Patton Escarpment	California margin	32.4	-120.6	3707	4	43.8	12.1	2.59E-06	3.2	0.9	This study
Site BC-10	California margin	32.5	-120.0	3800	4	46.3	8.5	2.59E-06	3.4	0.6	(*19*)
MANOP site S	North Pacific	11.0	-140.0	4910	4	19.7	3.0	2.59E-06	1.4	0.2	(*19*)

Note: 1) We adopted a bottom water temperature of 25 ºC for the shallow East China Sea shelf based on long-term observation in summer (*62*). For slope-deep sea sites, we assume a uniform T of 4 ºC.
2) This reflects the maximum gradient of pore-water [Be] to the sediment surface (bottom water). No bottom water Be concentrations were measured at the Mexico-California margin; for these sites, we thus used the bottom water [Be] in the Patton Escarpment (Site BC-10) from (*19*). The choice of this concentration (30 pM) is reasonable because deep sea [Be] is relatively stable, e.g. 28 pM in the North Pacific (*55*).
3) D_{Be}^{sed}: Be diffusion coefficients in sediment adjusted for bottom water temperature (*36*). Diffusive Be flux here is calculated using Eq. (1).
4) The uncertainty of the diffusive flux is propagated from that of the Be gradient.

Table S4. Comparison between globally-representative and our studied range of key environmental variables.

Variable[1,2,3]	Unit	0-0.2 km		0.2-4 km		>4 km		Reference	
		Globe	Study region[4]	Globe	Study region[4]	Globe	Study region[4]	Globe	Study region[4]
Water depth	km	*0.065* (0-0.2)	(0.012-0.046)	*2.8* (0.2-4)	(1.3-3.7)	*4.9* (4->10)	4.9	(*37*)	\
Sedimentation rate[5]	mg/cm^2/yr	*496*	*380* (200-5000)	1.73 ± 1.73	(3-15)	1.08 ± 0.97	(0.06-<0.6)	0-0.2 km: (*37, 63*); >0.2 km: (*64*)	(*65*); (*26*); (*66*)
Org. C rain rate	mmol C/m^2/d	*13.4*	15.2 (4.4-42.7)	*1.4*	(0.5-2.5)	*0.16*	0.13 ± 0.11	(*67*)	(*68*); (*26*); (*69*)
Org. C remineralization rate	mmol C/m^2/d	*9.4*	8.4 (3.6-17.6)	*1.2*	(0.4-1.3)	*0.15*	0.13 ± 0.11[6]	(*67*)	(*68*); (*26*); (*69*)

Note: 1) The value of each environmental variable is displayed as its average value ± standard deviation (minimum-maximum). As the data were reported in different forms in literature, certain statistical parameters are not applicable and thus not shown in some cases.
2) These variables on sedimentary and diagenetic environments are chosen because they might modulate benthic sedimentary Be fluxes.
3) Parameter values in italic indicate area-weighted average values.
4) The range of values represents that in the study region (East China Sea shelf, Californian margin or deep North Pacific) chosen for spatial extrapolation (Table S5). References for each study region are listed as: 0-0.2 km; 0.2-4 km; >4 km.
5) The area-weighted sedimentation rate on global shelves is calculated using the empirical relationship between water depth and sedimentation rate (in cm/yr) (*63*), a bulk dry density (1.2 g/cm^3) identical to that in the study region (*20*), and the bathymetry (*37*). The average sedimentation rate and its uncertainty at depths > 0.2 km over global scale are sourced from globally compiled ^{230}Th normalized sedimentary mass flux data (*64*). The sedimentation rate of the study region at >4 km (~1-<10 mm/kyr; (*66*)) is converted to mg/cm^2/yr using a depth-integrated bulk dry density of ~0.6 g/cm^3 (*70*).
6) The organic carbon remineralization rate (remineralization rate = rain rate - burial rate) in the study region at >4 km is set to be equal to the measured rain rate, as the organic carbon burial rate is estimated to be <0.001 mmol C/m^2/d (*69*).

Table S5. First-order estimate of oceanic Be budget

Be source or sink	[Be]	Material flux	Contributing area[10]	Be input or output	Proportion	Reference[1]
	pmol/kg	kg/yr	km^2	10^7 mol/yr	%	
River dissolved load[1,2,3]	514 ± 104	3.6E+16	9.8E+07	1.8 ± 0.4	26%	(*57*), Table S6, (*14*)
Eolian dust[1,2,4]	2.0E+07	(4.4 ± 0.3)E+11	3.6E+08	0.9 ± 0.06	12%	(*38*), (*39*), (*13*)
Benthic flux (shelf)[5,8]	140.0 ± 107.3 pmol/cm^2/yr		2.7E+07	3.8 ± 2.9	52%	This study
Benthic flux (0.2-4 km depths)[6,8]	2.9 ± 0.3 pmol/cm^2/yr		1.4E+08	0.4 ± 0.02	6%	This study
Benthic flux (>4 km depths)[7,8]	1.4 ± 0.2 pmol/cm^2/yr		1.9E+08	0.3 ± 0.03	4%	(*19*)
Be source (total)[11]				7.2 ± 2.9	100%	
Be sink (sediment burial)[9,11]			3.6E+08	6.9 ± 1.7	\	(*41*), (*10*)

Note: 1) The references for river or dust source are listed as: material flux, [Be], delivery efficiency to the oceans.

2) [Be] here is calculated by accounting for the corresponding Be delivery efficiency (estuarine transmission of 44%; dust solubility of 9%).

3) The relative uncertainty of riverine [Be] is estimated as the $(Be)_{riv\text{-}diss}$ flux-weighted relative standard deviation of [Be] from the compiled dataset in Table S6.

4) The material flux for dust is calculated from the average value and the standard deviation of three model results presented in (38) and compiled by (*71*).

5) The shelf benthic flux (pmol/cm^2/yr) is represented by the advection-dominated flux (using Eq. 3) on the East China Sea shelf (details in "Materials and Methods"). The flux uncertainty is derived from the standard deviation of Be gradients at these stations and the uncertainty on water exchange rate (Fig. S1).

6) The benthic flux (0.2-4 km) is estimated by the diffusion-dominated flux in the California margin. To obtain this value, we use the average diffusive flux from three stations at 1300-3707 m with non-anoxic conditions. The flux uncertainty is derived from the standard deviation of the fluxes at these stations.

7) The benthic flux (>4 km) and its uncertainty are estimated using the diffusion-dominated flux at a station in the deep North Pacific (4910 m; (*19*)).

8) The global benthic ^{9}Be input is 4.5×10^{7} mol/yr, accounting for only ~0.9% of the total riverine sediment-derived ^{9}Be input (5.3×10^{9} mol/yr) (*57, 61*).
9) The sediment burial output of ^{9}Be is calculated by dividing the atmospheric ^{10}Be input to the oceans, that is, the product of global grid-average ^{10}Be depositional flux in atoms/km^{2}/yr (*41*) and ocean area in km^{2}, by the global ocean area-weighted deep-ocean $^{10}Be/^{9}Be$ ratio (*10*) following the approach of (*40*). The uncertainty of the ^{9}Be burial flux reflects propagated uncertainties of both parameters.
10) The contributing area refers to the global drainage area for river dissolved load (*57*) or ocean area for other sources and the sink (*37*).
11) The mismatch between oceanic fluxes of the sources and the sink of Be is <10% and falls within the uncertainty.

Table S6. Compilation of global riverine dissolved Be concentration data

River Basin	Reference	Water discharge m^3/yr	$[Be]_{diss}$ pmol/L	$[Be]_{diss}$ SD[1] pmol/L
Amazon	(*13, 72, 73*)	6.46E+12	1049	219
Orinoco	(*73*)	1.13E+12	923	341
Ganges	(*13*)	4.92E+11	42	
Yangtze	(*72*)	9.27E+11	128	
Congo	(*72*)	1.23E+12	3824	625
Pearl	(*74, 75*)	1.67E+11	233	9
Mackenzie	(*52*)	2.84E+11	316	
Ob	(*52*)	4.26E+11	1598	
Yenisey	(*52*)	6.24E+11	317	
Lena	(*52*)	6.02E+11	1176	
Hudson	(*75*)	1.50E+10	2000	
Columbia	(*75*)	1.80E+10	353	
Fraser	(*75*)	8.60E+10	1055	49
Pitt	(*75*)	1.70E+09	215	
Santa Ana	(*75*)	7.40E+07	187	
Cosumnes	(*75*)	4.50E+08	2340	
Mokelunne	(*75*)	9.10E+08	1980	
Stanislas	(*75*)	7.30E+08	87	
Deer Creek	(*75*)	3.50E+07	686	
Merced	(*75*)	5.60E+08	261	
Klamath	(*75*)	3.70E+09	233	
Teviot	(*76*)[2]	6.19E+08	2219	
Tweed	(*76*)[2]	2.51E+09	2219	
L. Swale	(*76*)[2]	6.46E+08	4439	
Ure	(*76*)[2]	6.47E+08	2219	
Nidd	(*76*)[2]	4.65E+08	3329	
Ouse	(*76*)[2]	1.52E+09	2219	
Wharf	(*76*)[2]	5.46E+08	2219	
Derwent	(*76*)[2]	5.47E+08	2219	
Aire	(*76*)[2]	1.15E+09	2219	
Calder	(*76*)[2]	5.62E+08	3329	
Don	(*76*)[2]	1.77E+08	5548	
Trent	(*76*)[2]	2.86E+09	2219	
Upper River Severn	(*77*)	1.67E+07	8877	
Vörå creek	(*78*)	1.12E+08	269363	11848
Awe	(*14*)	1.80E+09	494	
Etive	(*14*)	4.00E+08	610	
Krka	(*14*)	1.50E+09	92	
Zrmanja	(*14*)	1.20E+09	54	

Continued below

Summary		
Parameter	**Unit**	**Value**
Sum of discharge	m^3/yr	1.25E+13
Discharge-weighted $[Be]_{diss}$	pmol/L	1167
Global water discharge	m^3/yr	3.60E+13
Global $(Be)_{riv\text{-}diss}$ flux[3]	mol/yr	4.20E+07
$(Be)_{riv\text{-}diss}$ flux (post-estuary)[4]	mol/yr	*1.85E+07*
Flux-weighted uncertainty[5]	mol/yr	*3.76E+06*

Note: 1) If $[Be]_{diss}$ data of multiple samples (spatial/temporal replicates) are available, we calculate the average value and the standard deviation (SD) in Columns "$[Be]_{diss}$" and "$[Be]_{diss}$ SD", respectively.
2) Data in (*76*) was originally reported in units of μg/L and thus its precision is likely close to ~0.01 μg/L (~1 nM).
3) Global riverine dissolved Be flux is calculated using the global water discharge (*57*) and the discharge-weighted $[Be]_{diss}$ of our compiled dataset.
4) Riverine dissolved Be flux after estuarine scavenging is calculated using a global-average scavenging efficiency of 56% (*14*).
5) The relative uncertainty of riverine dissolved Be flux (post-estuary) is calculated using the existing data on relative standard deviation of $[Be]_{diss}$ (Column "$[Be]_{diss}$ SD") weighted by their riverine Be flux.

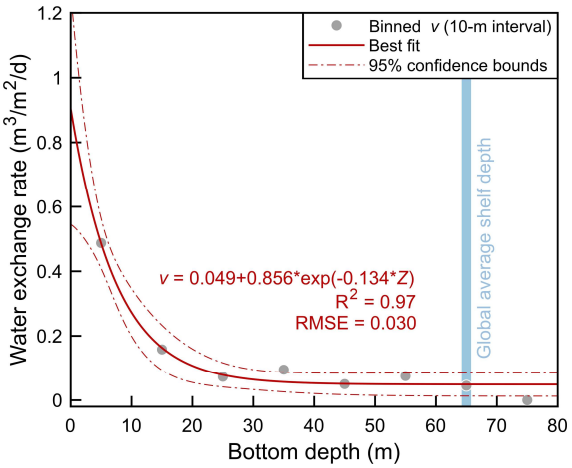

Figure S1 Relationship between bottom water depth (Z) and water exchange rate (v) on continental shelves. Water exchange rate data in the literature were derived from $^{224}Ra/^{228}Th$ disequilibria in China coastal seas (*33*). Data were binned at 10 m depth interval and fitted using an exponential equation following (*33*). Note that the literature data (*33*) were re-processed here in order to derive an estimate of uncertainty (red dashed lines) on v, which was not available in the original paper. At global average shelf depth, the water exchange rate is 0.049 ± 0.036 $m^3/m^2/d$. The uncertainty on v represents the overall deviation from the best-fit equation and takes the regional heterogeneity of v into account.

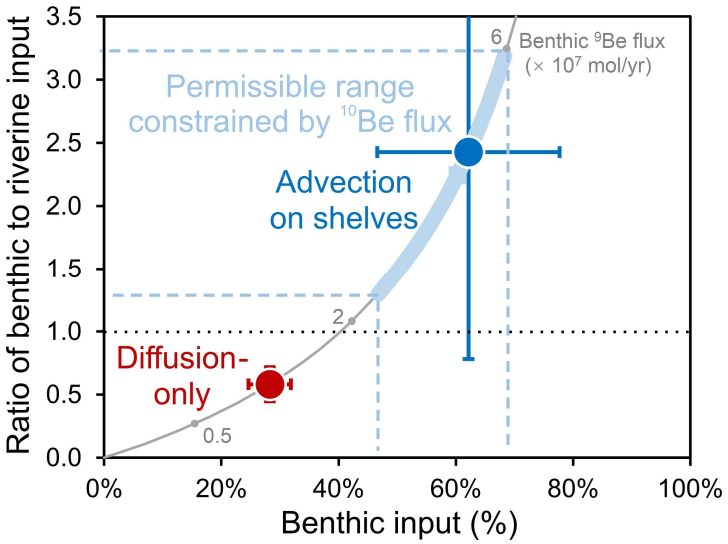

Figure S2 Sensitivity of benthic ^{9}Be input (% of the total input; X axis) and ratio of benthic to riverine ^{9}Be input (Y axis) to different scenarios on benthic flux calculation. Error bars include all the uncertainties propagated from every ^{9}Be source or sink. The permissible range constrained by the ^{10}Be flux (light blue band) indicates the range of benthic ^{9}Be fluxes ($4.2 \pm 1.7 \times 10^{7}$ mol/yr) calculated from input-output balance of ^{9}Be, that is, the difference between the total ^{9}Be output (constrained by the global atmospheric ^{10}Be input and the global average deep-sea ^{10}Be/^{9}Be; Table S5) and non-benthic ^{9}Be sources (river and dust; Table S5). This permissible range of benthic ^{9}Be flux is then converted to a range of paired X-Y values by comparing to fluxes of other non-benthic sources. The benthic ^{9}Be flux calculated by only diffusion processes (i.e. advection on shelves not included; red circle) accounts for 28% of the total input and corresponds to ~60% of the riverine dissolved input. However, this estimate does not fall within the permissible range of the benthic source. In comparison, the benthic ^{9}Be flux that takes advection processes on shelves into account (dark blue circle) agrees well with the permissible range. Note that even when considering the large flux uncertainty related to estimates on water advection, the total benthic flux is close to, or higher than, the riverine dissolved input (minimum ratio: 0.8; average ratio: 2.4), and accounts for 62% ± 16% of the total ^{9}Be input.

REFERENCES AND NOTES

1. J. W. B. Rae, Y. G. Zhang, X. Liu, G. L. Foster, H. M. Stoll, R. D. M. Whiteford, Atmospheric CO_2 over the past 66 million years from marine archives. *Annu. Rev. Earth Planet. Sci.* **49**, 609–641 (2021).

2. J. Zachos, M. Pagani, L. Sloan, E. Thomas, K. Billups, Trends, rhythms, and aberrations in global climate 65 Ma to present. *Science* **292**, 686–693 (2001).

3. M. E. Raymo, W. F. Ruddiman, Tectonic forcing of Late Cenozoic climate. *Nature* **359**, 117–122 (1992).

4. S. Misra, P. N. Froelich, Lithium isotope history of Cenozoic seawater: Changes in silicate weathering and reverse weathering. *Science* **335**, 818–823 (2012).

5. R. A. Berner, K. Caldeira, The need for mass balance and feedback in the geochemical carbon cycle. *Geology* **25**, 955–956 (1997).

6. M. A. Torres, A. J. West, G. Li, Sulphide oxidation and carbonate dissolution as a source of CO_2 over geological timescales. *Nature* **507**, 346–349 (2014).

7. J. K. Caves, A. B. Jost, K. V. Lau, K. Maher, Cenozoic carbon cycle imbalances and a variable weathering feedback. *Earth Planet. Sci. Lett.* **450**, 152–163 (2016).

8. J. K. Caves, D. E. Ibarra, F. von Blanckenburg, Neogene cooling driven by land surface reactivity rather than increased weathering fluxes. *Nature* **571**, 99–102 (2019).

9. J. K. Willenbring, F. von Blanckenburg, Long-term stability of global erosion rates and weathering during late-Cenozoic cooling. *Nature* **465**, 211–214 (2010).

10. F. von Blanckenburg, J. Bouchez, River fluxes to the sea from the ocean's $^{10}Be/^{9}Be$ ratio. *Earth Planet. Sci. Lett.* **387**, 34–43 (2014).

11. K. Deng, H. Wittmann, F. von Blanckenburg, The depositional flux of meteoric cosmogenic ^{10}Be from modeling and observation. *Earth Planet. Sci. Lett.* **550**, 116530 (2020).

12. F. von Blanckenburg, J. Bouchez, D. E. Ibarra, K. Maher, Stable runoff and weathering fluxes into the oceans over Quaternary climate cycles. *Nat. Geosci.* **8**, 538–542 (2015).

13. E. T. Brown, C. I. Measures, J. M. Edmond, D. L. Bourlès, G. M. Raisbeck, F. Yiou, Continental inputs of beryllium to the oceans. *Earth Planet. Sci. Lett.* **114**, 101–111 (1992).

14. T. J. Suhrhoff, J. Rickli, K. Crocket, E. Bura-Nakic, D. Vance, Behavior of beryllium in the weathering environment and its delivery to the ocean. *Geochim. Cosmochim. Acta* **265**, 48–68 (2019).

15. S. Li, S. L. Goldstein, M. E. Raymo, Neogene continental denudation and the beryllium conundrum. *Proc. Natl. Acad. Sci. U.S.A.* **118**, e2026456118 (2021).

16. F. von Blanckenburg, J. Bouchez, J. K. Willenbring, D. E. Ibarra, J. K. C. Rugenstein, There is no Neogene denudation conundrum. *Proc. Natl. Acad. Sci. U.S.A.* **119**, e2202387119 (2022).

17. V. A. Elrod, W. M. Berelson, K. H. Coale, K. S. Johnson, The flux of iron from continental shelf sediments: A missing source for global budgets. *Geophys. Res. Lett.* **31**, L12307 (2004).

18. A. N. Abbott, B. A. Haley, J. McManus, C. E. Reimers, The sedimentary flux of dissolved rare earth elements to the ocean. *Geochim. Cosmochim. Acta* **154**, 186–200 (2015).

19. D. L. Bourlès, G. Klinkhammer, A. C. Campbell, C. I. Measures, E. T. Brown, J. M. Edmond, Beryllium in marine pore waters: geochemical and geochronological implications. *Nature* **341**, 731–733 (1989).

20. J. P. Liu, A. C. Li, K. H. Xu, D. M. Velozzi, Z. S. Yang, J. D. Milliman, D. J. DeMaster, Sedimentary features of the Yangtze River-derived along-shelf clinoform deposit in the East China Sea. *Cont. Shelf Res.* **26**, 2141–2156 (2006).

21. J. Zhu, Z. Zhu, J. Lin, H. Wu, J. Zhang, Distribution of hypoxia and pycnocline off the Changjiang Estuary, China. *J. Mar. Sys.* **154**, 28–40 (2016).

22. S. T. Lennartz, A. Lehmann, J. Herrford, F. Malien, H. P. Hansen, H. Biester, H. W. Bange, Long-term trends at the Boknis Eck time series station (Baltic Sea), 1957–2013: Does climate change counteract the decline in eutrophication? *Biogeosciences* **11**, 6323–6339 (2014).

23. F. Scholz, J. McManus, S. Sommer, The manganese and iron shuttle in a modern euxinic basin and implications for molybdenum cycling at euxinic ocean margins. *Chem. Geol.* **355**, 56–68 (2013).

24. E. Seibold, N. Exon, M. Hartmann, F.-C. Kögler, H. Krumm, G. Lutze, R. Newton, F. Werner, Marine geology of Kiel bay, in *Sedimentology of Parts of Central Europe, Guidebook VIII International Sedimentology Congress* (Kramer, 1971).

25. C. A. Nittrouer, G. R. Lopez, L. Donelson Wright, S. J. Bentley, A. F. D'Andrea, C. T. Friedrichs, N. I. Craig, C. K. Sommerfield, Oceanographic processes and the preservation of sedimentary structure in Eckernförde Bay, Baltic Sea. *Cont. Shelf Res.* **18**, 1689–1714 (1998).

26. J. McManus, W. M. Berelson, S. Severmann, R. L. Poulson, D. E. Hammond, G. P. Klinkhammer, C. Holm, Molybdenum and uranium geochemistry in continental margin sediments: Paleoproxy potential. *Geochim. Cosmochim. Acta* **70**, 4643–4662 (2006).

27. S. Bruggmann, S. Severmann, J. McManus, Geochemical conditions regulating chromium preservation in marine sediments. *Geochim. Cosmochim. Acta* **348**, 239–257 (2023).

28. W. M. Berelson, J. McManus, K. H. Coale, K. S. Johnson, T. Kilgore, D. Burdige, C. Pilskaln, Biogenic matter diagenesis on the sea floor: A comparison between two continental margin transects. *J. Mar. Res.* **54**, 731–762 (1996).

29. D. Bourlès, G. M. Raisbeck, F. Yiou, ^{10}Be and ^{9}Be in marine sediments and their potential for dating. *Geochim. Cosmochim. Acta* **53**, 443–452 (1989).

30. H. Wittmann, F. von Blanckenburg, J. Bouchez, N. Dannhaus, R. Naumann, M. Christl, J. Gaillardet, The dependence of meteoric ^{10}Be concentrations on particle size in Amazon River bed sediment and the extraction of reactive ^{10}Be/^{9}Be ratios. *Chem. Geol.* **318–319**, 126–138 (2012).

31. F. Scholz, J. Cheng, Z. Zhang, P. Vosteen, C. Siebert, M. Frank, Benthic-pelagic coupling and isotopic fractionation of barium in Kiel Bight, SW Baltic Sea. *Front. Mar. Sci.* **10**, 1101095 (2023).

32. J. McManus, W. M. Berelson, S. Severmann, K. S. Johnson, D. E. Hammond, M. Roy, K. H. Coale, Benthic manganese fluxes along the Oregon-California continental shelf and slope. *Cont. Shelf Res.* **43**, 71–85 (2012).

33. X. Shi, L. Wei, Q. Hong, L. Liu, Y. Wang, X. Shi, Y. Ye, P. Cai, Large benthic fluxes of dissolved iron in China coastal seas revealed by $^{224}Ra/^{228}Th$ disequilibria. *Geochim. Cosmochim. Acta* **260**, 49–61 (2019).

34. D. E. Hammond, C. Fuller, in *The use of radon-222 to estimate benthic exchange and atmospheric exchange rates in San Francisco Bay* (American Association for the Advancement of Science-Pacific Division, 1979).

35. D. Archer, A. Devol, Benthic oxygen fluxes on the Washington shelf and slope: A comparison of in situ microelectrode and chamber flux measurements. *Limnol. Oceanogr.* **37**, 614–629 (1992).

36. B. P. Boudreau, in *Diagenetic Models and Their Implementation* (Springer, Berlin, 1997), vol. 410.

37. B. Eakins, G. Sharman, Hypsographic curve of Earth's surface from ETOPO1 (NOAA National Geophysical Data Center, Boulder, CO, 2012).

38. T. D. Jickells, Z. S. An, K. K. Andersen, A. R. Baker, G. Bergametti, N. Brooks, J. J. Cao, P. W. Boyd, R. A. Duce, K. A. Hunter, H. Kawahata, N. Kubilay, J. laRoche, P. S. Liss, N. Mahowald, J. M. Prospero, A. J. Ridgwell, I. Tegen, R. Torres, Global iron connections between desert dust, ocean biogeochemistry, and climate. *Science* **308**, 67–71 (2005).

39. R. L. Rudnick, S. Gao, 3.01 - Composition of the Continental Crust A2 - Holland, Heinrich D, in *Treatise on Geochemistry*, K. K. Turekian, Ed. (Pergamon, Oxford, 2003), pp. 1–64.

40. F. von Blanckenburg, R. K. O'Nions, N. S. Belshaw, A. Gibb, J. R. Hein, Global distribution of beryllium isotopes in deep ocean water as derived from Fe Mn crusts. *Earth Planet. Sci. Lett.* **141**, 213–226 (1996).

41. U. Heikkilä, F. von Blanckenburg, The global distribution of Holocene meteoric 10Be fluxes from atmospheric models. Distribution maps for terrestrial Earths surface applications (GFZ Data Services, GFZ Potsdam, Germany, 2015).

42. T. L. Ku, M. Kusakabe, C. I. Measures, J. R. Southon, G. Cusimano, J. S. Vogel, D. E. Nelson, S. Nakaya, Beryllium isotope distribution in the western North Atlantic: A comparison to the Pacific. *Deep Sea Res. Part A Oceanogr. Res. Papers* **37**, 795–808 (1990).

43. R. F. Anderson, Y. Lao, W. S. Broecker, S. E. Trumbore, H. J. Hofmann, W. Wolfli, Boundary scavenging in the Pacific Ocean: A comparison of ^{10}Be and ^{231}Pa. *Earth Planet. Sci. Lett.* **96**, 287–304 (1990).

44. G. M. Patton, R. Francois, D. Weis, E. Hathorne, M. Gutjahr, M. Frank, K. Gordon, An experimental investigation of the acquisition of Nd by authigenic phases of marine sediments. *Geochim. Cosmochim. Acta* **301**, 1–29 (2021).

45. F. Herman, D. Seward, P. G. Valla, A. Carter, B. Kohn, S. D. Willett, T. A. Ehlers, Worldwide acceleration of mountain erosion under a cooling climate. *Nature* **504**, 423–426 (2013).

46. K. G. Miller, M. A. Kominz, J. V. Browning, J. D. Wright, G. S. Mountain, M. E. Katz, P. J. Sugarman, B. S. Cramer, N. Christie-Blick, S. F. Pekar, The Phanerozoic record of global sea-level change. *Science* **310**, 1293–1298 (2005).

47. B. A. Haley, J. Du, A. N. Abbott, J. McManus, The impact of benthic processes on rare earth element and neodymium isotope distributions in the oceans. *Front. Mar. Sci.* **4**, 426 (2017).

48. A. Bernhardt, M. Oelze, J. Bouchez, F. von Blanckenburg, M. Mohtadi, M. Christl, H. Wittmann, ^{10}Be/^{9}Be ratios reveal marine authigenic clay formation. *Geophys. Res. Lett.* **47**, e2019GL086061 (2020).

49. H. Wittmann, F. von Blanckenburg, M. Mohtadi, M. Christl, A. Bernhardt, The competition between coastal trace metal fluxes and oceanic mixing from the ^{10}Be/^{9}Be ratio: Implications for sedimentary records. *Geophys. Res. Lett.* **44**, 8443–8452 (2017).

50. K. Deng, S. Yang, J. Du, E. Lian, D. Vance, Dominance of benthic flux of REEs on continental shelves: Implications for oceanic budgets. *Geochem. Perspect. Lett.* **22**, 26–30 (2022).

51. Y. Sohrin, S. Urushihara, S. Nakatsuka, T. Kono, E. Higo, T. Minami, K. Norisuye, S. Umetani, Multielemental determination of GEOTRACES key trace metals in seawater by ICPMS after preconcentration using an ethylenediaminetriacetic acid chelating resin. *Anal. Chem.* **80**, 6267–6273 (2008).

52. M. Frank, D. Porcelli, P. Andersson, M. Baskaran, G. Björk, P. W. Kubik, B. Hattendorf, D. Guenther, The dissolved Beryllium isotope composition of the Arctic Ocean. *Geochim. Cosmochim. Acta* **73**, 6114–6133 (2009).

53. T. J. Suhrhoff, J. Rickli, M. Christl, E. G. Vologina, V. Pham, M. Belhadj, E. V. Sklyarov, C. Jeandel, D. Vance, Source to sink analysis of weathering fluxes in Lake Baikal and its watershed based on riverine fluxes, elemental lake budgets, REE patterns, and radiogenic (Nd, Sr) and $^{10}Be/^{9}Be$ isotopes. *Geochim. Cosmochim. Acta* **321**, 133–154 (2022).

54. J. McManus, W. M. Berelson, G. P. Klinkhammer, D. E. Hammond, C. Holm, Authigenic uranium: Relationship to oxygen penetration depth and organic carbon rain. *Geochim. Cosmochim. Acta* **69**, 95–108 (2005).

55. M. Kusakabe, T. L. Ku, J. R. Southon, J. S. Vogel, D. E. Nelson, C. I. Measures, Y. Nozaki, Distribution of ^{10}Be and ^{9}Be in the Pacific Ocean. *Earth Planet. Sci. Lett.* **82**, 231–240 (1987).

56. P. J. Statham, P. A. Yeats, W. M. Landing, Manganese in the eastern Atlantic Ocean: Processes influencing deep and surface water distributions. *Mar. Chem.* **61**, 55–68 (1998).

57. J. D. Milliman, K. L. Farnsworth, in *River Discharge to the Coastal Ocean – a Global Synthesis* (Cambridge Univ. Press, 2011).

58. B. Campforts, V. Vanacker, J. Vanderborght, S. Baken, E. Smolders, G. Govers, Simulating the mobility of meteoric ^{10}Be in the landscape through a coupled soil-hillslope model (Be2D). *Earth Planet. Sci. Lett.* **439**, 143–157 (2016).

59. J. Gaillardet, J. Viers, B. Dupré, Trace Elements in River Waters, in *Treatise on Geochemistry*, H. D. Holland, K. K. Turekian, Eds. (Elsevier, Oxford, ed. 2, 2014), pp. 195–235.

60. C. Shen, J. Beer, P. Kubik, W. Sun, T. Liu, K. Liu, ^{10}Be in desert sands, falling dust and loess in China. *Nucl. Instrum. Methods Phys. Res., Sect. B* **268**, 1050–1053 (2010).

61. F. von Blanckenburg, J. Bouchez, H. Wittmann, Earth surface erosion and weathering from the ^{10}Be (meteoric)/^{9}Be ratio. *Earth Planet. Sci. Lett.* **351–352**, 295–305 (2012).

62. C.-T. A. Chen, Chemical and physical fronts in the Bohai, Yellow and East China seas. *J. Mar. Sys.* **78**, 394–410 (2009).

63. J. J. Middelburg, K. Soetaert, P. M. J. Herman, Empirical relationships for use in global diagenetic models. *Deep Sea Res. Part I* **44**, 327–344 (1997).

64. K. M. Costa, C. T. Hayes, R. F. Anderson, F. J. Pavia, A. Bausch, F. Deng, J.-C. Dutay, W. Geibert, C. Heinze, G. Henderson, C. Hillaire-Marcel, S. Hoffmann, S. L. Jaccard, A. W. Jacobel, S. S. Kienast, L. Kipp, P. Lerner, J. Lippold, D. Lund, F. Marcantonio, D. McGee, J. F. McManus, F. Mekik, J. L. Middleton, L. Missiaen, C. Not, S. Pichat, L. F. Robinson, G. H. Rowland, M. Roy-Barman, A. Tagliabue, A. Torfstein, G. Winckler, Y. Zhou, ^{230}Th normalization: New insights on an essential tool for quantifying sedimentary fluxes in the modern and quaternary ocean. *Paleoceanogr. Paleoclimatol.* **35**, e2019PA003820 (2020).

65. B. Deng, J. Zhang, Y. Wu, Recent sediment accumulation and carbon burial in the East China Sea. *Global Biogeochem. Cycles* **20**, GB3014 (2006).

66. S. Emerson, V. Grundmanis, D. Graham, Carbonate chemistry in marine pore waters: MANOP sites C and S. *Earth Planet. Sci. Lett.* **61**, 220–232 (1982).

67. D. J. Burdige, Preservation of organic matter in marine sediments: Controls, mechanisms, and an imbalance in sediment organic carbon budgets? *Chem. Rev.* **107**, 467–485 (2007).

68. G. Song, S. Liu, Z. Zhu, W. Zhai, C. Zhu, J. Zhang, Sediment oxygen consumption and benthic organic carbon mineralization on the continental shelves of the East China Sea and the Yellow Sea. *Deep Sea Res. Part II* **124**, 53–63 (2016).

69. W. M. Berelson, D. E. Hammond, D. O'Neill, X. m. Xu, C. Chin, J. Zukin, Benthic fluxes and pore water studies from sediments of the central equatorial north Pacific: Nutrient diagenesis. *Geochim. Cosmochim. Acta* **54**, 3001–3012 (1990).

70. D. Kadko, A multitracer approach to the study of erosion in the northeast equatorial Pacific. *Earth Planet. Sci. Lett.* **63**, 13–33 (1983).

71. N. M. Mahowald, A. R. Baker, G. Bergametti, N. Brooks, R. A. Duce, T. D. Jickells, N. Kubilay, J. M. Prospero, I. Tegen, Atmospheric global dust cycle and iron inputs to the ocean. *Global Biogeochem. Cycles* **19**, GB4025 (2005).

72. C. I. Measures, J. M. Edmond, The geochemical cycle of ^{9}Be: A reconnaissance. *Earth Planet. Sci. Lett.* **66**, 101–110 (1983).

73. E. T. Brown, J. M. Edmond, G. M. Raisbeck, D. L. Bourlès, F. Yiou, C. I. Measures, Beryllium isotope geochemistry in tropical river basins. *Geochim. Cosmochim. Acta* **56**, 1607–1624 (1992).

74. W. Kong, L. Zhou, G. Aumaître, D. Bourlès, K. Keddadouche, Dissolved and particulate beryllium isotopes in the Pearl River estuary: Their geochemical behavior in estuarine water and potential contributions from anthropogenic sources. *Front. Mar. Sci.* **8**, 689890 (2021).

75. M. Kusakabe, T. L. Ku, J. R. Southon, L. Shao, J. S. Vogel, D. E. Nelson, S. Nakaya, G. L. Cusimano, Be isotopes in rivers/estuaries and their oceanic budgets. *Earth Planet. Sci. Lett.* **102**, 265–276 (1991).

76. C. Neal, Dissolved and acid available particulate beryllium in eastern UK surface waters. *Sci. Total Environ.* **314–316**, 185–208 (2003).

77. C. Neal, Dissolved beryllium in rainfall, stream and shallow groundwaters in the Upper River Severn catchments, Plynlimon, mid Wales. *Sci. Total Environ.* **314–316**, 171–184 (2003).

78. M. E. Åström, C. Yu, P. Peltola, J. K. Reynolds, P. Österholm, M. I. Nystrand, A. Augustsson, J. J. Virtasalo, L. Nordmyr, A. E. K. Ojala, Sources, transport and sinks of beryllium in a coastal landscape affected by acidic soils. *Geochim. Cosmochim. Acta* **232**, 288–302 (2018).